Optimal reconstruction of attractors from experimental time series by the wavering product

W.-D. Sponheimer and C. Wilke
Department of Physics, Ernst-Moritz-Arndt University, Domstrasse 10a, D-17489 Greifswald, Germany
(Received 29 August 1996)

In this work the dynamics of a periodically excited neon glow discharge is examined by determining a Lyapunov exponent spectrum from the discharge current. Therefore it is necessary to reconstruct an attractor with the Takens delay coordinate method [F. Takens, in *Dynamical Systems and Turbulence*, edited by D. Rand and L.-S. Young, Lecture Notes in Mathematics Vol. 898 (Springer, Berlin, 1981), p. 366] from the discharge current topologically correct. For a simultaneous determination of both the embedding dimension and the delay time the wavering product is used here as an efficient method. [S1063-651X(97)06405-2]

PACS number(s): 05.45.+b

I. INTRODUCTION

In complex systems such as plasmas, beside temporal and spatial turbulences there exist nonlinear processes with few degrees of freedom. Deterministic chaos in gas discharge plasmas has been proved in many experiments so far. In former researches in the nonlinear dynamics of periodically excited neon glow discharges periodicity, two- and three-frequency quasiperiodicity and low-dimensional chaos could be observed [1]. A differentiation of the observed three-frequency attractors into quasiperiodicity and chaos was possible by determining the autocorrelation function, the K_2 entropy, and the correlation dimension from the experimental time series. In many experiments certainly the chaos is extremely weak, so that a distinction between chaos and three-frequency quasiperiodicity is often difficult, as Linsay and Cumming observed [2,3]. By determining a Lyapunov exponent spectrum (LES) from the corresponding experimental time series it is possible to distinguish between periodic, quasiperiodic, and chaotic attractors reliably. Besides, the strength of the chaos could be quantified by the LES because the Lyapunov exponents represent a measure for the average exponential divergence or convergence of two neighboring trajectories. In addition, the Kolmogorov-Sinaj entropy [4] and the Kaplan-Yorke dimension [5] could easily be calculated from the LES. Therefore, statements of the transport properties of systems can be made as well [6]. The LES and other attractor properties depend strongly from the choice of the phase-space reconstruction. Therefore, it is decisive to find suitable reconstruction parameters. In a former work the smallest topologically correct embedding dimension of the attractor was determined by the false nearest-neighbor method [7]. Another method for testing the topological properties of the attractor represents the wavering product. It determines the smallest possible embedding dimension and allows the choice of a convenient delay time additionally. The wavering product was tested for driven nonlinear systems successfully in this work. For nearly-noise-free time series, good results were obtained with the wavering product. Furthermore, the precision of the calculated LES is dependent on the details of the applied algorithm and the values of its input parameters. Moreover, there is the difficulty that many algorithms depend sensitively on noise in experimental time series. The algorithm for determining a LES from time series presented here is based on the concepts of Eckmann *et al.* [8] and Sano and Sawada [9] and is improved in some details. In this procedure the linearized phase flow mapping is deduced from the temporal evolution of a next-neighbor area around reference points on the attractor and approximated by the method of least squares. After the algorithm has been described, it is explored on which parameter interval of the algorithm the LES of a Lorenz system converges and the calculated LES is compared with literature data. In this way we find out how to limit the parameter space in order to get optimal results from the algorithm. Then the tested algorithm is applied to experimental time series, which have been obtained by sampling the discharge current of a periodically excited neon glow discharge. Periodic and chaotic attractors as well as three tori can be identified definitely with this algorithm for a noise level less than 2%. The results obtained are confirmed by a comparison with other methods of time-series analysis such as Poincaré section, Fourier spectrum, and autocorrelation function.

II. RECONSTRUCTION OF THE ATTRACTOR

In most cases only one characteristic quantity of the experiment is obtained as a time series. Then a trajectory through an m-dimensional phase space is reconstructed from this time series. The dimension of the phase space is determined by the number of degrees of freedom of an unknown nonlinear differential equation system that describes the phase-space dynamics. (The expression ''degrees of freedom,'' which is often used as follows, means the degrees of freedom of the phace space and not the degrees of freedom of motion of the many-particle system plasma.) According to the concept of delay time coordinates that was proposed by Takens [10], the data $x_i = x(i\Delta t)$, $i = 0, \ldots, N-1$, sampled with equidistant time steps Δt are reconstructed into phase-space vectors as

$$\vec{x}_i = (x_i, x_{i+m}, x_{i+2m}, \ldots, x_{i+(d_e-1)m}).$$

The reconstruction is valid for an embedding dimension $d_e > 2D_k + 1$ and in the case of infinite data points $N \to \infty$ even for arbitrary delay times $\tau = m\Delta t$ [11]. D_k is the capacity dimension of the attractor. This is a sufficient condition. There exist possibly lower embedding dimensions. In the

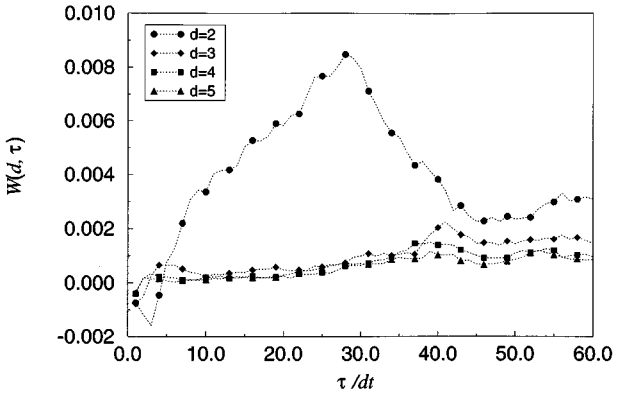

FIG. 1. Wavering product of the Van der Pol system without noise versus delay time. Dimensions are varying from 2 to 5.

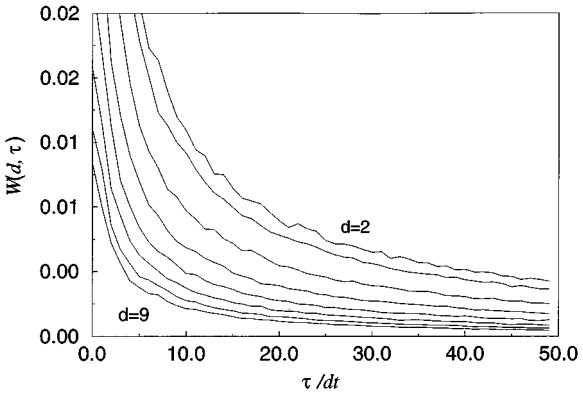

FIG. 3. Wavering product of a stochastic third order-autoregressive process. Dimensions are varying from 2 to 9.

case of time series with a finite number of data there is no arbitrary choice of the delay time possible because the properties of the reconstructed attractor depend sensitively on τ. Therefore, procedures have to be found to allow both the choice of a suitable embedding dimension and a convenient delay time. Yet it makes sense to choose d_e as small as possible because, on the one hand, it reduces the computing time for analyses of the reconstructed attractor such as correlation dimension and LES and, on the other hand, the LES will not be falsified by the determination of false Lyapunov exponents, which appear if the embedding dimension is overestimated; see, e.g., [12].

The range of suitable delay times can be reduced on the time interval $0<\tau<0.5T_c$. T_c is the characteristic recurrence time of the system. In the first instance τ need not be so small that the attractor is nearly reduced on the hyperdiagonal of the phase space. However, a delay time $>T_c$ would lead to an overfolding of the attractor. But there still exist bad reconstructions of some attractors even within this range of τ. To further restrict this range of convenient delay times there exist several methods. An early method to find a suitable delay time is based on the correlation of coordinates [13]. As a delay time the time interval is used here at which a correlation of the first two coordinates does not occur anymore. That means that τ is the time at which the autocorrelation function first becomes zero. This procedure works well for two-dimensional systems. Yet for higher-dimensional systems the correlation of the other coordinates is not taken into account. Another method to obtain convenient delay times is to calculate the correlation dimension D_2 and search for a region that remains constant at a variance of τ [14].

Other methods have been developed to find a minimal embedding. In the opinion of Froehling *et al.* [15] the smallest integer dimension above the fractal dimension is sufficient as the embedding dimension for physical systems. That corresponds just to very simply structured attractors. The single-valued system approach as stated by Broomhead and King [16] determines the minimal embedding by a singular-valued decomposition of the trajectory matrix. Because it is a linear procedure, only statements about the linear independence of the coordinates can be made. Another procedure is to find the number of initial conditions for a definite reconstruction of the attractor [17]. Buzug and Pfister [18] use two complementary methods to determine both the embedding dimension and the delay time. The fill factor algorithm presents a measure for the global use of the phase space by the attractor. The second method, which is called local deformation, allows one to recognize intersections in the attractors trajectories. Another work that concerns with the determination of LES from time series that are obtained from the discharge current of an undriven argon discharge plasma [19] applies the false next-neighbor method [7]. This procedure

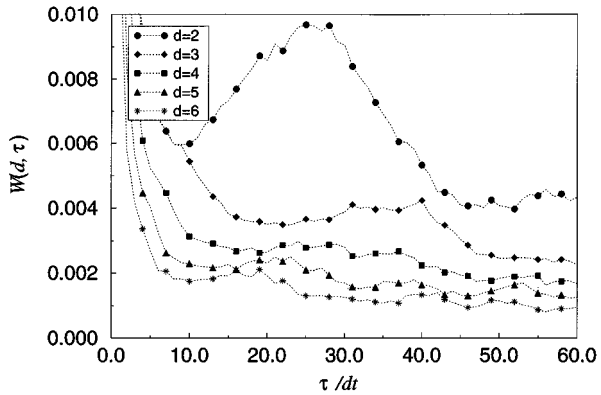

FIG. 2. Wavering product of the Van der Pol system with 2% Gaussian noise versus delay time. Dimensions are varying from 2 to 6.

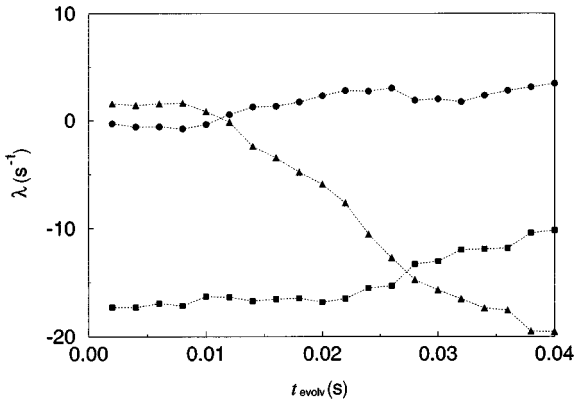

FIG. 4. Lyapunov exponent spectrum versus the time range for the linear approximation of the flow map for the Lorenz system.

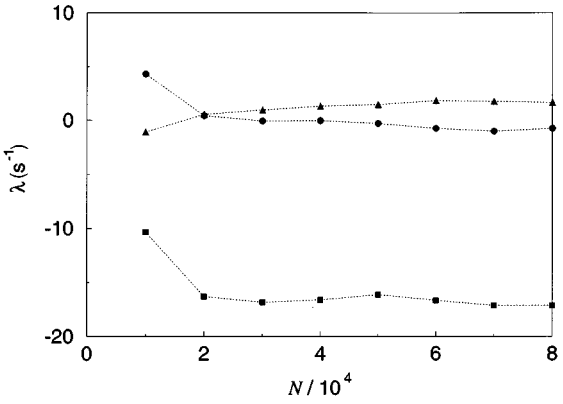

FIG. 5. Lyapunov exponent spectrum versus the number of data points that the attractor contains.

looks into the topological changes of an area on the attractor when the embedding dimension is increased. Since this method does not determine the delay time, the time when the autocorrelation function of the time series has sloped to $1/e$ is taken as the delay time $\tau = m\Delta t$.

Contrary to these methods that require usually two procedures to obtain embedding dimension and delay time, both parameters can simultaneously be determined by the wavering product. The wavering product was developed by Liebert [20] and is described in the following section.

A. Wavering product

A transition from a sufficient embedding dimension into a higher dimension can be regarded as a topological mapping. The wavering product makes good use of this. A topological mapping transforms an enclosed region into another enclosed region. That means that the neighboring points of a reference point on a sufficient embedded attractor keep preserved if the embedding dimension increases, whereas in a not sufficient embedded attractor the distance between neighboring points and reference point may become very large if the dimension is increased. Then the reconstructed attractor is only a projection of the real attractor onto a subspace and the trajectory intersects with itself at least once. These contents can be expressed in the formula

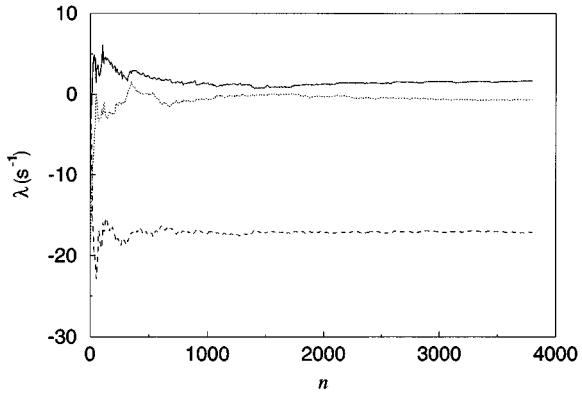

FIG. 6. Lyapunov exponent spectrum versus the number of reference points.

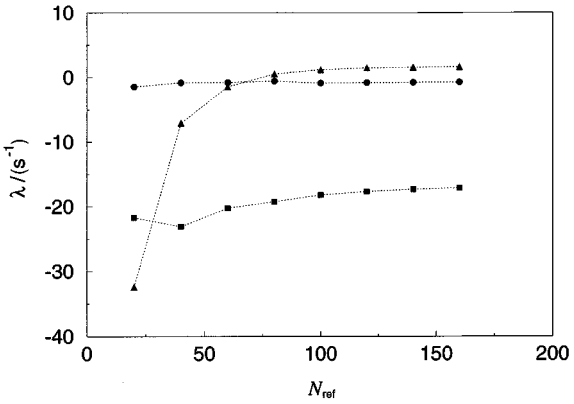

FIG. 7. Lyapunov exponent spectrum versus the number of next neighbors.

$$Q_1(i,k,m,\tau) = \frac{l^{\tau}_{m+1}(i,j(k,m))}{l^{\tau}_{m+1}(i,j(k,m+1))}.$$

$l^{\tau}_{m+1}(i,j(k,m))$ is the distance between the reference point i and its kth next neighbor of embedding m when embedded in dimension $m+1$. $l^{\tau}_{m+1}(i,j(k,m+1))$ is the distance between the reference point i and its kth next neighbor of embedding $m+1$ when embedded in dimension $m+1$. This expression is of value 1 if the kth next neighbor of point i is represented by the same point in both dimensions. If the embedding is not sufficient and the neighboring point is placed at a region on the attractor far away from the reference point while incrementing the embedding dimension, the expression becomes much larger than one. If the wavering product remains one for all higher embedding dimensions, the embedding is correct. Because the trajectory intersects with itself just at few positions on the attractor, the average over the attractor has to be taken.

Another problem arises from the fact that a reconstruction with the delay coordinates method does not preserve the order of next neighbors around a reference point if the embedding dimension is increased. A geometrical average is taken to compensate this wavering effect:

$$P_i(m,\tau) = \left(\prod_{k=1}^{p} Q_1(i,k,m,\tau) \right)^{1/p}.$$

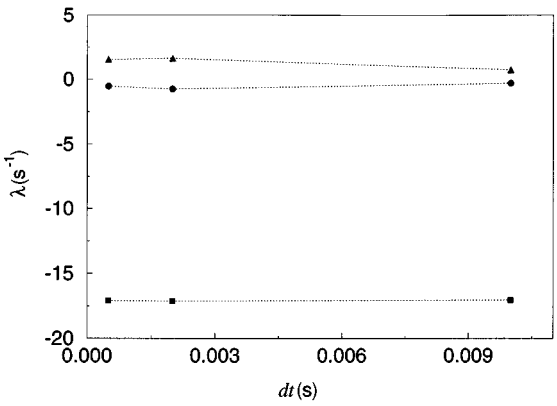

FIG. 8. Lyapunov exponent spectrum versus the sampling time.

TABLE I. Theoretical and calculated properties observed from the Lorenz attractor.

	λ_1	λ_2	λ_3	K_2	D_{KY}
Theoretical	1.50	0.00	−22.46	1.50	2.06
Calculated	1.43±0.15	−0.27±0.25	−16.91±0.48	1.43	2.06

The wavering effect can be amplified by noise. Therefore, the number p of next neighbors has to exceed at least the noise level. Because of border effects the improved wavering product still does not converge near enough to one. This influence of border effects can be compensated by an additional term

$$Q_2(i,k,m,\tau)=\frac{l_m^\tau(i,j(k,m))}{l_m^\tau(i,j(k,m+1))}.$$

The wavering product then becomes

$$w_i(m,\tau)=\left(\prod_{k=1}^{p} Q_1(i,k,m,\tau)Q_2(i,k,m,\tau)\right)^{1/p}.$$

As stated above, the wavering product is averaged over the attractor. An average over 5–10% of the data points proved sensible. In the case of sufficient embedding there exists a τ dependence, which is compensated by the factor $1/\tau$. The logarithmic wavering product converges against zero:

$$W(m,\tau)=\frac{1}{\tau}\ln\langle w_i(m,\tau)\rangle_i.$$

B. Test of the wavering product on driven systems

Since the analysis of time series is focused on driven discharges, it is reasonable to test the wavering product algorithm for a driven nonlinear test system. The Van der Pol equation was established recently for modeling the dynamics of a driven low-pressure glow discharge [21]. So this system seemed to be suitable for a test of the wavering product. The following parameter values were selected, which determine a chaotic regime of the Van der Pol system:

$$\frac{\partial^2}{\partial t^2}x(t)-\mu\omega_0[1-x(t)^2]\frac{\partial}{\partial t}x(t)+\omega_0^2x(t)=p\cos(\omega_1 t),$$

$$\mu=5,\quad \omega_0=1,\quad \omega_1=2.465,\quad p=5.$$

Figure 1 shows the wavering product of the selected system. The underlying time series consists of 40 000 points and the wavering product was averaged over 40 next neighbors. Obviously W converges against embedding dimension $d=3$ over a wide range of delay times τ.

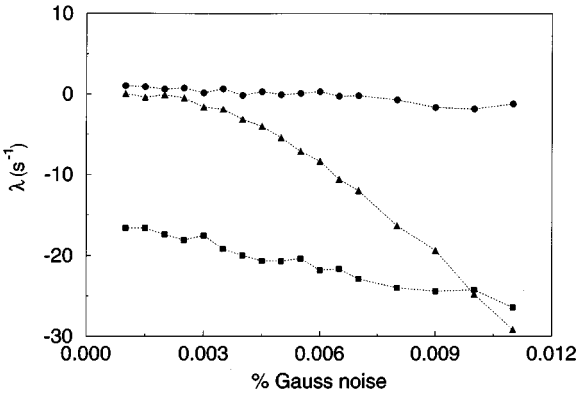

FIG. 9. Lyapunov exponent spectrum versus the Gaussian noise that is imposed on the time series.

Figure 2 shows the wavering product for the same system with 2% Gaussian noise added. In this case convergence is more indistinct than in the case of the noiseless system. But there is still a great gap between $d=2$ and $d=3$. From that the conclusion can be made that additional noise in time series lets the wavering product converge to higher embedding dimensions above the minimal embedding. Therefore, noise in time series should be reduced before an analysis with the wavering product.

Furthermore, the question should be answered if the wavering product can distinguish between stationary random processes and deterministic processes because Fredkin and Rice obtained a random second-order autoregressive process beeing estimated as deterministic by the false nearest-neighbor method [22]. In order to determine if the wavering product suffers from the same problem a third-order autoregressive process was generated, satisfying the equation

$$x(t)=1.59x(t-1)-1.2x(t-2)+0.6x(t-3)+u(t),$$

with a white-noise sequence $u(t)$. Figure 3 shows the convergence of the wavering product for this process. Because the computing time grows rapidly with the embedding dimension, the wavering product was restricted to maximum dimension $d=9$ here. However, the wavering product seems to converge regularly against zero for high embedding dimensions, as one would expect, since a stochastic process is infinite dimensional in phase space. Obviously the wavering product is not ''fooled'' by a stationary random process of that smoothness contrary to the method of nearest neighbors.

TABLE II. Experimental parameters and discovered dimensions for all the observed regimes. ν assigns the external drive frequency, p_0 is the pressure in the discharge tube, I_0 is the direct current portion of the discharge current, and α represents the modulation amplitude.

Dynamic regime	ν (kHz)	p_0 (torr)	I_0 (mA)	α	D_2	D_{KY}
Periodic	3.113	1.7	10.0	0.05	0.95±0.05	
Quasiperiodic	4.063	1.7	10.0	0.04	3.05±0.05	
Chaotic	5.020	1.7	15.0	0.05	3.60±0.05	5.56

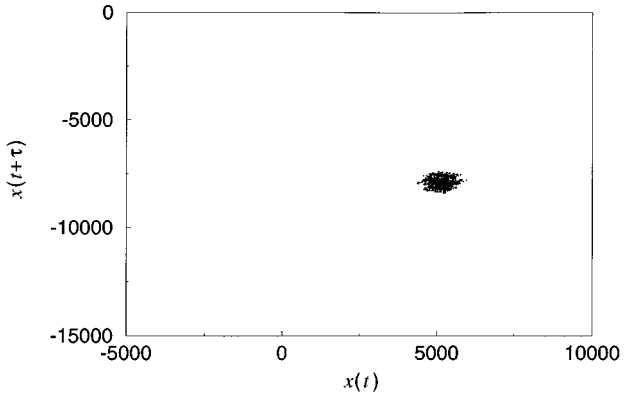

FIG. 10. Poincaré section through the periodic attractor.

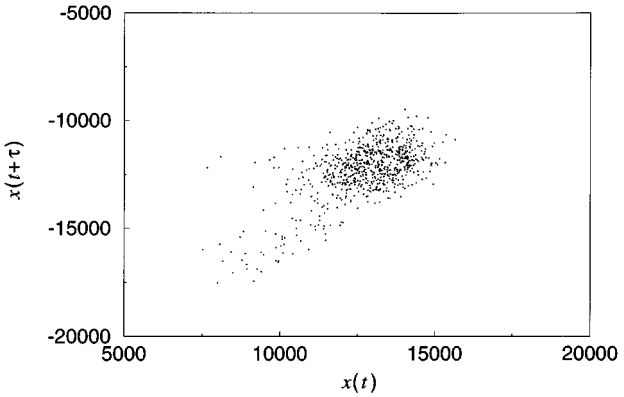

FIG. 12. Poincaré section through the chaotic attractor.

III. THE LYAPUNOV EXPONENT SPECTRUM

A Lyapunov exponent spectrum is an important quantity to classify and quantify dynamical systems. The decision whether a time series is periodic, quasiperiodic, or chaotic can be made by calculating a Lyapunov exponent spectrum because it is characteristic for special dynamical states. Lyapunov exponents state how the phase flow mapping transforms an infinitesimal ϵ sphere on the attractor into an ellipse in the average of time:

$$\lambda_k = \lim_{t\to\infty} \frac{1}{t} \int_0^t \ln \gamma_k dt.$$

The γ_k are the eigenvalues of the linearized phase flow mapping.

A. Algorithm for the calculation of Lyapunov exponents

The algorithm to calculate Lyapunov exponents presented here corresponds in its essential features to the method developed by Sano and Sawada [9]. Moreover, the local tangent mappings T^i at position i of the phase flow are approximated by the method of least squares. This happens in the following manner. For a reference point $\vec{x}_i$ the n next neighbors on the attractor are determined with respect to the Euclidian distance. To prevent the next-neighbor area from expanding so much that a linear approximation is not possible an ϵ sphere around $\vec{x}_i$ can be given. Thus only the next neighbors within the ϵ sphere are taken into account. The tangent mapping T^i is approximated into a matrix $A^{i,m}$ by the method of least squares [9]. m assigns the number of time steps for the linear mapping. Applying the mapping p times on a coordinate base results in a product matrix $\Pi_{j=i}^{i+p} A^{j,m}$. This sequence of linear mappings allows the coordinate axes to converge into the direction of the biggest Lyapunov exponent enforced by the dynamics of the system. It is therefore necessary to reorthonormalize the coordinate base. Sano and Sawada propose a Gram-Schmid reorthonormalization procedure [23]. The algorithm used here decomposes the matrix $A^{j,m}$ into an orthogonal and an upper triangular matrix with positive diagonal elements [8,24] as

$$\begin{aligned} A^{1,m}\underline{\underline{1}} &= Q^{1,m}R^{1,m}, \\ A^{2,m}A^{1,m}\underline{\underline{1}} &= Q^{2,m}R^{2,m}R^{1,m}, \\ &\vdots \\ \prod_{j=1}^{p} A^{j,m} &= Q^{p,m}\prod_{j=1}^{p} R^{j,m}. \end{aligned}$$

Hence the tangent mapping $A^{j,m}$ is represented by an orthonormal system that is rotated by $Q^{j-1,m}$ against the canonical coordinate base $\underline{\underline{1}}$ at the beginning of the sequence. Because this orthonormal system nearly corresponds to the principal

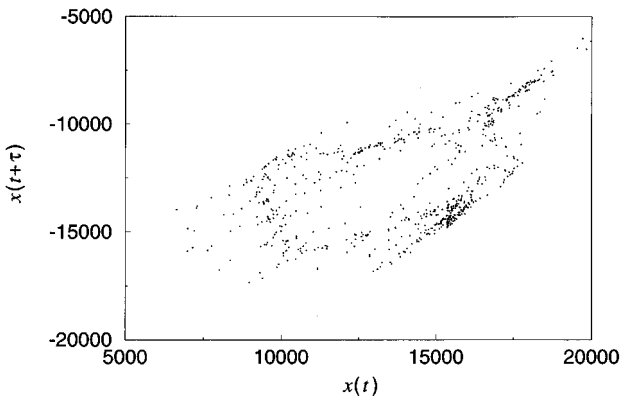

FIG. 11. Poincaré section through the three-frequency quasiperiodic attractor.

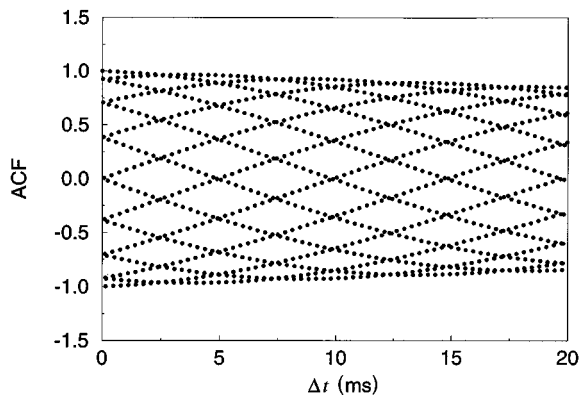

FIG. 13. Autocorrelation function of the periodic attractor.

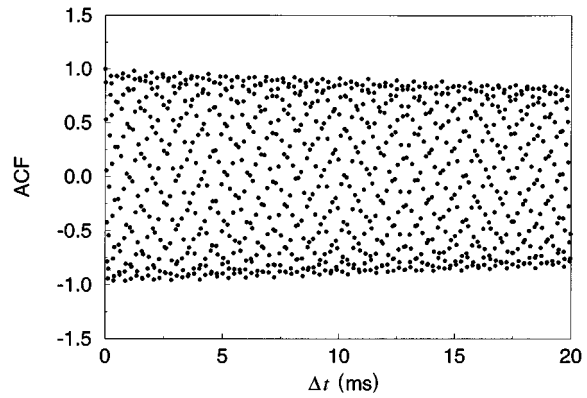

FIG. 14. Autocorrelation function of the quasiperiodic attractor.

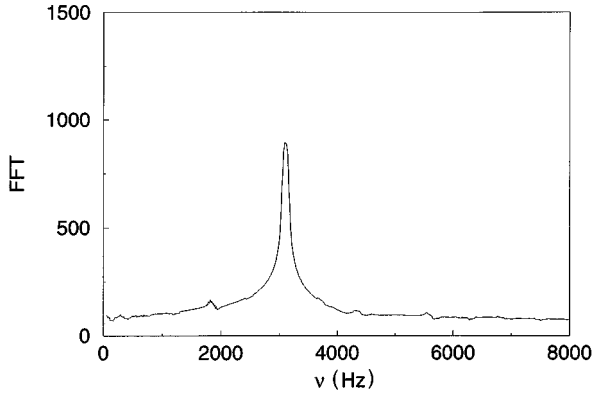

FIG. 16. Power spectrum of the periodic attractor.

axes system of the tangent mapping $A^{j,m}$, the Lyapunov exponents can be calculated from the diagonal elements of the upper triangular matrix with good approximation:

$$\lambda_i = \frac{1}{pm\Delta t} \sum_{j=1}^{p} \ln(R^{j,m})_{ii}.$$

The procedure described above begins at several randomly partitioned positions on the attractor to include each part of the attractor and to guarantee a good spatial average of the Lyapunov exponents. The first q tangent mappings were not taken into account for the calculations because the arbitrary base at the start of the procedure takes some time to train on the principal axes system. During this time the algorithm would deliver inaccurate results.

B. Optimization and test of the algorithm

The reconstructed attractor $\vec{x}_i$ represents the phase flow of a dynamical system in discrete time steps. It depends on the choice of the reconstruction parameters embedding dimension d_e and delay time τ whether the attractor approximates the system well. In addition, the density and the amount of information that the reconstructed attractor contains about the phase flow are given by the sampling rate, the precision, and the total amount of data of the obtained time series. It was found that time series with high sampling frequencies were needed for a reliable determination of negative Lyapunov exponents (at least 100 points per orbit) [25], whereas for the determination of positive Lyapunov exponents attractors with many orbits are required (at least 100 orbits). To fulfill both requirements large amounts of data are needed. The used time series usually contained of 80 000 data and had a precision of 12 bits.

The input parameters of the above described algorithm will now be optimized and then the algorithm will be tested on a Lorenz system. The algorithm contains many parameters. The parameter space has to be reduced in a sensible manner so that the algorithm delivers optimal results. For that purpose an area in parameter space is selected where the LES remains constant. The parameter dependence of the LES is shown here for a Lorenz system,

$$\dot{x} = \sigma(y - x),$$

$$\dot{y} = cx - y - xz,$$

$$\dot{z} = -bz + xy,$$

with $\sigma = 16$, $b = 4.0$, and $R = 45.92$ (Figs. 4–9). Constant parameters were set as follows: evolution time $\Delta t_{\text{evol}} = 0.008$, number of points $N = 80\,000$, step width $dt = 0.002$ (which corresponds to about 250 points per orbit), number of reference points $N_{\text{ref}} = 3500$, and number of next neighbors $n = 160$. N has to be proportional to n when N is varied to keep the radius of the next-neighbor sphere around a reference point nearly constant.

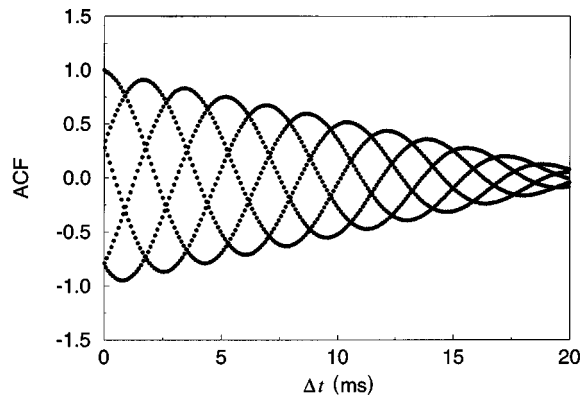

FIG. 15. Autocorrelation function of the chaotic attractor.

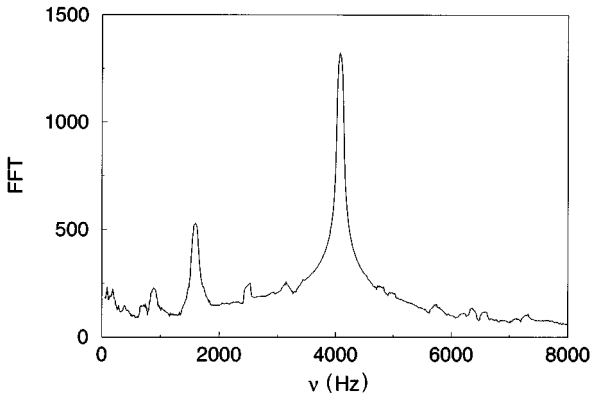

FIG. 17. Power spectrum of the quasiperiodic attractor.

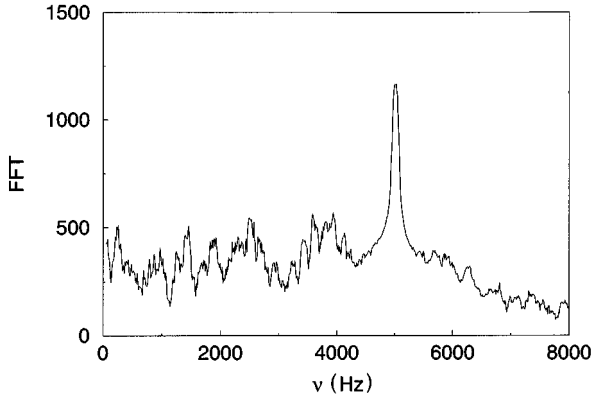

FIG. 18. Power spectrum of the chaotic attractor.

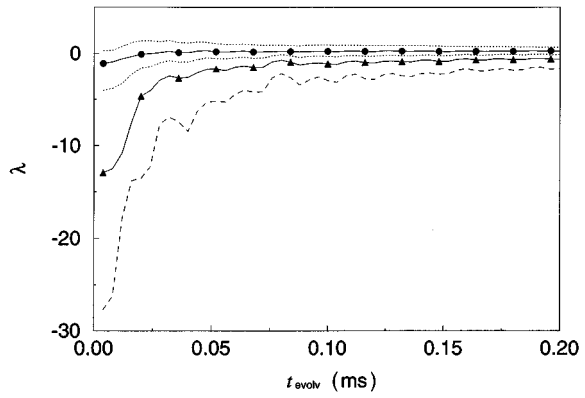

FIG. 20. Lyapunov exponent spectrum for the quasiperiodic system.

Convergence could be achieved for all varied parameters. Figure 4 shows a convergence of the LES for evolution times $\Delta t_{\mathrm{evol}}<0.01$ s, corresponding to 50 points per orbit. Hence step widths less than 0.01 s must be taken. For experimentally obtained time series the step width is given by the inverse sampling frequency $dt=\nu^{-1}$. Because of a better statistics the LES converges for large values of N, N_{ref}, and n, as Figs. 5–7 show. But n may not become too large; otherwise, the ϵ sphere exceeds the range for a linear approximation of the $\vec{F}$ map. The influence of the step width on the LES can be neglected if only step widths within the convergent range of the evolution time are considered (Fig. 8). Against that there is a strong dependence of the LES on the noise level, as demonstrated in Fig. 9. There is Gaussian noise superimposed on the Lorenz attractor. The noise level relative to the horizontal extent of the attractor is displayed on the abscissa of Fig. 9. As can be recognized from Fig. 9, the algorithm delivers reasonable results until the noise level gets across 2%. Hence the noise in the experimental time series has to be reduced at least under this level. Further investigations on the influence of interactive noise to the LES are made in [26].

The Lyapunov exponents of the Lorenz system that are calculated in the convergent range of all parameters are compared with published data [25] in Table I. Error bars refer to the fluctuations of the Lyapunov exponents within the convergence region. It is shown that the calculated Lyapunov exponents are in good agreement with the theoretical values within the error bars, with exception of the negative one. Since $\|\lambda_-\|$ is huge against λ_+, the next neighbors contract much faster in the λ_- direction as they expand in the λ_+ direction. If a part of the next neighbors contracts in the λ_- direction under the noise level or goes down under the data precision, λ_- will be systematically overestimated. The LES converges on different regions in parameter space for each system. These regions have to be found for each system individually.

IV. ANALYSIS OF EXPERIMENTAL TIME SERIES

Time series that were obtained by sampling the discharge current of a neon glow discharge with a 500-kHz sampling frequency were analyzed. The experimental setup is described in detail in [27]. Various dynamical regimes can be set there by varying the frequency that drives the discharge. The following analysis refers to a periodic, a quasiperiodic, and a chaotic time series, which were sampled at experimental conditions, as given in Table II.

As a first step the noise contained in the time series had to be reduced. This could be realized by a method that interpolates a time series through cubic splines and then averages over them. This procedure is applied in [19] as well. Then a Poincaré section, a Fourier spectrum, and an autocorrelation function were derived from the low-noise time series to classify their dynamics (Figs. 10–18). Moreover, by the calcula-

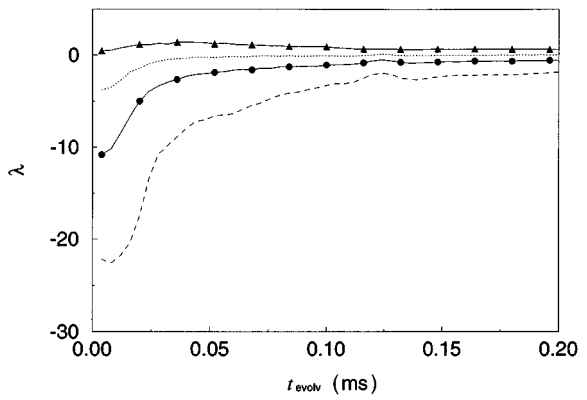

FIG. 19. Lyapunov exponent spectrum for the periodic system.

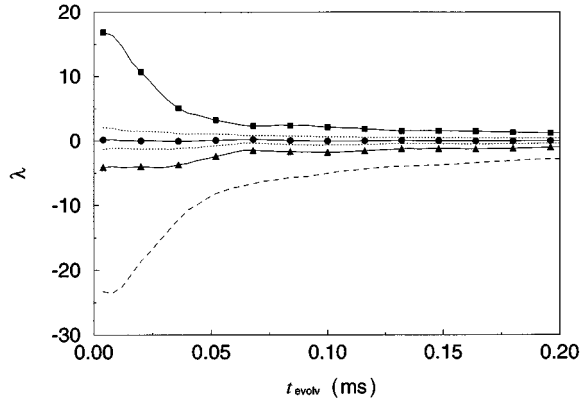

FIG. 21. Lyapunov exponent spectrum for the chaotic system.

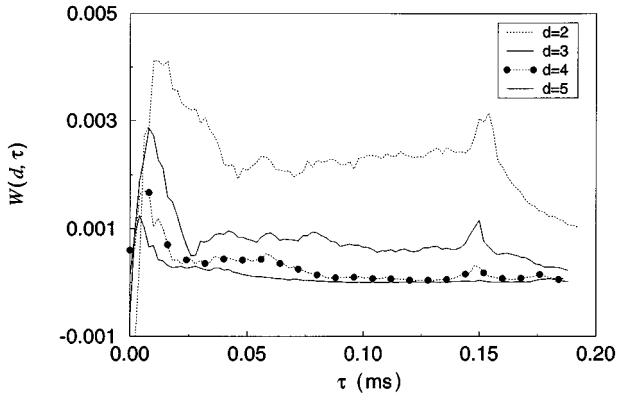

FIG. 22. Wavering product for the periodic system.

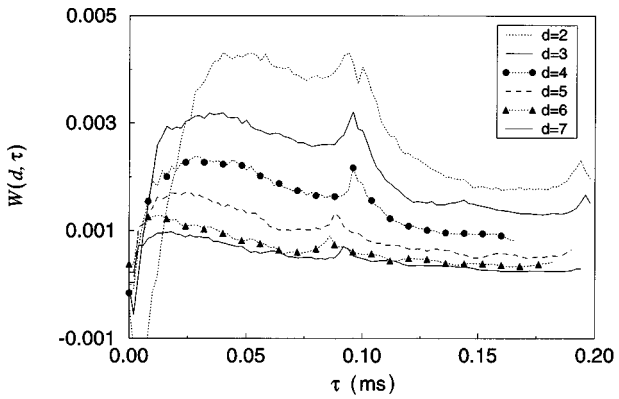

FIG. 24. Wavering product for the chaotic system.

tion of the correlation dimension D_2, which can easily be done with the Grassberger-Procaccia algorithm [28] (delay time$=1/3T$, Table II), dynamical regimes of the time series can now be determined. Hence the first time series corresponds to a one-period, the second time series corresponds to a three-torus (quasiperiodic), and the third is chaotic. This could be verified with a LES, which was obtained by applying the above-described algorithm onto the time series.

Figures 19–21 show the LES against the evolution time. The LES for the three time series is represented schematically as $(0,-,-,-)$, $(0,0,0,-,-)$ and $(+,+,0,-,-,-)$ within the error bars, corresponding to a periodic, a quasiperiodic and a chaotic state. This scheme refers to the convergence region of the LES for evolution times $\Delta t_{\mathrm{evol}}<10^{-2}$ ms. The errors of the LES are estimated by the fluctuations of the convergence niveaus. The innermost Lyapunov exponents even converge until $\Delta t_{\mathrm{evol}}=0.04$ ms. For a more precise determination of the Lyapunov exponents smaller evolution times are needed. This would require higher sampling rates, which could not be realized experimentally.

In Figs. 22–24 the wavering products for the three time series are shown. They depend on the parameters delay time τ and embedding dimension of the attractor d_e. In the case of the periodic and the quasiperiodic system convergence against zero can clearly be recognized since the embedding dimension $d=4$ and $d=5$. The corresponding delay times were set to $\tau=0.082$ ms and $\tau=0.074$ ms. Yet in the case of the chaotic system the convergence is more indistinct and the convergence is situated above zero. As demonstrated in Sec. II B, the insufficient convergence is related to a remaining part of noise contained in the time series that could not be reduced further. This noise can be seen in the Fourier spectrum of the chaotic time series as well (Fig. 18). On the other hand, the application of the noise reduction algorithm implicates the risk of deforming chaotic trajectories and therefore alters the dynamics of the system essentially, as stated in [19]. Thus a noise level less than 2% was tolerated so that reliable Lyapunov exponents could be determined. Because of the insufficient convergence of the wavering product, the chaotic attractor that is reconstructed with parameters $d_e=6$ and $\tau=0.062$ ms is possibly embedded too high. Hence the LES would contain d_e-d_r additional false Lyapunov exponents besides d_r true Lyapunov exponents. d_r represents the real embedding dimension of the attractor corresponding to the system's number of degrees of freedom. If an embedding dimension $d_e=4$ is considered to be as sufficient for the chaotic system and the second and fourth Lyapunov exponent is deleted from the LES, the Lyapunov dimension is equivalent to the correlation dimension within the error bars.

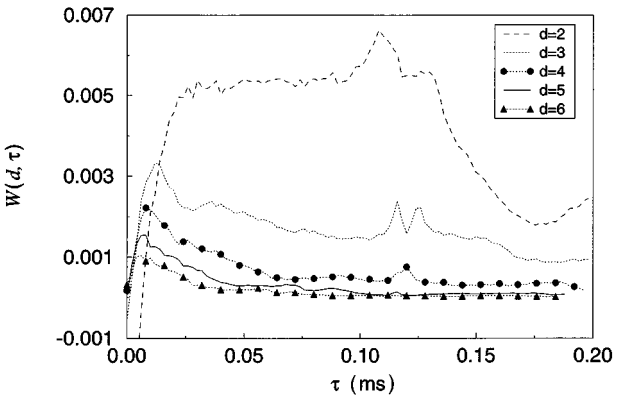

FIG. 23. Wavering product for the quasiperiodic system.

V. CONCLUSION

An algorithm for the calculation of LES from time series has been presented that allows for the determination of negative Lyapunov exponents. The algorithm has been tested on a Lorenz system and has been optimized with respect to its parameters. For sensible parameter settings good agreement could be achieved between the results of the algorithm and literature values of the model system. Then with the algorithm a LES has been found from the discrete discharge current of a periodically excited neon glow discharge. Therefore, an attractor had to be reconstructed from the experimental time series with its reconstruction parameter's embedding dimension and delay time determined by the wavering product. Chaotic, periodic, and three-frequency quasiperiodic time behavior has been proved to be dependent on the external drive frequency. These results could be confirmed by further analyses with the Poincaré section, the Fourier spectrum, the correlation dimension, and the autocorrelation function. Because of the sensitivity of the LES algorithm and especially the wavering product to noise, the noise level of the time series under analysis had to be reduced. In

the case of the chaotic time series the noise level could only be reduced down to 2% because by a further noise reduction with the mentioned algorithm a change of the dynamic properties of the attractor seemed to be very likely. Though a noise level of 2% was not problematic for the LES algorithm, it probably let the wavering product overestimate the embedding dimension, as was assumed by a comparison between the Lyapunov dimension and correlation dimension. Together with a good noise reduction procedure, the LES algorithm presented in this work provides an efficient method to classify and quantify dynamical systems from experimental time series.

ACKNOWLEDGMENTS

We thank Stephan Gubsch, Jörg Schmeißel, and Klaus-Dieter Weltmann for experimental support and helpful discussions.

[1] B. Albrecht, H. Deutsch, R. W. Leven, and C. Wilke, Phys. Scr. **47**, 196 (1993).
[2] A. W. Cumming and P. S. Linsay, Phys. Rev. Lett. **60**, 2719 (1988).
[3] P. S. Linsay and A. W. Cumming, Physica D **40,** 196 (1989).
[4] A. N. Kolmogorov, Dokl. Akad. Nauk. SSSR **119**, 861 (1958).
[5] P. Fredrickson, J. L. Kaplan, E. D. Yorke, and J. A. Yorke, J. Differ. Eq. **49**, 185 (1983).
[6] P. Gaspard and G. Nicolis, Phys. Rev. Lett. **65**, 1693 (1990).
[7] M. B. Kennel, R. Brown, and H. D. I. Abarbanel, Phys. Rev. A **45**, 3403 (1992).
[8] J.-P. Eckmann, O. Kamphorst, D. Ruelle, and S. Ciliberto, Phys. Rev. A **34**, 4971 (1986).
[9] M. Sano and Y. Sawada, Phys. Rev. Lett. **55**, 1082 (1985).
[10] F. Takens, in *Dynamical Systems and Turbulence*, edited by D. Rand and L.-S. Young, Lecture Notes in Mathematics Vol. 898 (Springer, Berlin, 1981), p. 366.
[11] R. Mañé, in *Dynamical Systems and Turbulence* (Ref. [10]), p. 230.
[12] U. Parlitz, Int. J. Bif. Chaos **2**, 1 (1992).
[13] H. G. Schuster, *Deterministic Chaos* (VCH, Weinheim, 1988).
[14] A. Destexte, J. A. Sepulchre, and A. Babloyantz, Phys. Lett. A **132**, 101 (1988).
[15] H. Froehling, J. Crutchfield, D. Farmer, and N. Packard, Physica D **3**, 605 (1981).
[16] D. S. Broomhead and J. P. King, Physica D **20**, 217 (1986).
[17] A. Cenys and K. Pyragas, Phys. Lett. A **129**, 227 (1988).
[18] Th. Buzug and G. Pfister, Phys. Rev. A **45**, 7073 (1992).
[19] W. Huang, W. X. Ding, D. L. Feng, and C. X. Yu, Phys. Rev. E **50**, 1062 (1994).
[20] W. Liebert, *Chaos und Herzdynamik: Rekonstruktion und Charakterisierung Seltsamer Attraktoren aus Skalaren Chaotischen Zeitreihen* (Deutsch-Verlag, Frankfurt am Main, 1991).
[21] T. Klinger, A. Piel, F. Seddighi, and C. Wilke, Phys. Lett. A **182**, 312 (1993).
[22] Donald R. Fredkin and John A. Rice, Phys. Rev. E **51**, 2950 (1995).
[23] H. Boseck, *Einführung in die Theorie der Linearen Vektorräume*, 4th ed. (Deutscher Verlag der Wissenschaften, Berlin, 1981).
[24] J. Holzfuss and W. Lauterborn, Phys. Rev. A **39**, 2146 (1989).
[25] Alan Wolf, Jack B. Swift, Harry L. Swinney, and John A. Vastano, Physica D **16**, 285 (1985).
[26] Th.-M. Kruel, M. Eiswirth, and F. W. Schneider, Physica D **63**, 117 (1993).
[27] J. Schmeißel, Master thesis, Ernst-Moritz-Arndt-Universität Greifswald, 1996 (unpublished).
[28] P. Grassberger and I. Procaccia, Phys. Rev. Lett. **50**, 346 (1983).